Thin Solid Films 619 (2016) 102–111

Contents lists available at ScienceDirect

Thin Solid Films

journal homepage: www.elsevier.com/locate/tsf

Complementary photogating effect in microcrystalline silicon n-i-p structures

F.A. Rubinelli

Instituto de Desarrollo Tecnológico para la Industria Química (INTEC), Universidad Nacional del Litoral (UNL), CONICET, Güemes 3450, (3000) Santa Fe, Argentina

ARTICLE INFO

Article history:
Received 18 February 2016
Received in revised form 26 July 2016
Accepted 20 October 2016
Available online 23 October 2016

Keywords:
Photogating effect
Microcrystalline silicon
Solar sells
Optical detectors

ABSTRACT

Spectral responses above the unity at short wavelengths have not been yet reported in μc-Si:H based n-i-p devices illuminated with a red bias light. In solar cells this effect is known as the Complementary Photo-Gating Effect. After calibrating the input parameters of our computer code by matching experimental output device characteristics, the necessary conditions to predict these anomalous responses at short wavelengths were explored. In order to obtain SR higher than unity at short wavelengths in μc-Si:H n-i-p devices under red bias illumination a highly defective buffer layer must be present at the p/i interface. The short wavelength a.c. probe beam modulates the carrier concentration trapped at the gap states of the defective interface strengthen the electrical field in the intrinsic layer and weaken the electrical field inside the p-doped and p/i buffer layers. The short wavelength a.c. probe beam reduces the total recombination loss inside the intrinsic layer with respect to its counterpart under only red bias light illumination generating a net gain and spectral responses over unity. This phenomenon is predicted in devices with either high or low mobility (p)-layers, such as (p)-a-SiC:H and (p)-μc-Si:H respectively, that are not very efficiently doped with boron. Spectral responses higher than one are very sensitive to the electrical parameters of the p/i defective buffer such as mobility gap, thickness, density of defects, mobilities, capture cross sections of donor traps, and to the Boron density present in the p-layer and to the spectral content of the red bias light.

© 2016 Elsevier B.V. All rights reserved.

1. Introduction

Spectral Responses (SR) larger than unity in thin film devices have been reported by several researchers [1–12]. The observation of SR > 1, also known as anomalous responses, was first demonstrated in 1984 by Maruska et al. in light soaked hydrogenated amorphous silicon (a-Si:H) Schottky diodes by illuminating the front contact with a DC blue bias light [1] showing that the device can function as an optically controlled amplifier for small AC signals. The phenomenon was explained by the modulation of the series resistance present at the rear free field region of the Schottky barrier. Eight years later, Hou et al. using the computer code AMPS [2], predicted anomalous SR in degraded a-Si:H based p-i-n solar cells illuminating the device with a blue bias light for red probe beam wavelengths [3]. Hou et al. showed that the strongly absorbed blue bias light created a low-field region in the front part of the intrinsic layer near the p/i interface, while increasing the field in the back of the intrinsic layer. The red monochromatic light with a weaker flux generates holes throughout the device which, if trapped in sufficient numbers, results in an increase of the field in the front low-field region. This allows the release of blue bias light-produced carriers previously unable to traverse the front part of the device before recombining and feeding the current response of the probe beam at a different wavelength [3]. The phenomenon, called the Photo-Gating Effect (PGE) by the authors, was experimentally confirmed. It was not observed in as-deposited or annealed p-i-n samples.

The PGE was also reported by Rubinelli in forward biased a-Si:H Schottky barriers below the flat band condition [4], by C. Main in reverse biased light soaked a-Si:H based p-i-n junctions [5], and by H.B.T. Li et al. [8] and S·Reynolds et al. [9] in hydrogenated microcrystalline silicon (μc-Si:H) n-i-p and p-i-n solar cells respectively. Experimental evidence of the sensitivity of the PGE to the blue bias and probe beam intensities, intrinsic layer thickness and defect density, applied voltage were obtained [1–5,8]. Therefore a-Si:H and μc-Si:H based devices showing SR ≥ 1 can be used as photodiodes with internal gains. In the photovoltaic mode blocking contacts prevent the re-injection of photo-generated carriers [1–9]. Alternatively, in the photoconductive mode devices are forward biased beyond the flat band condition and gains greater than unity are associated with secondary photocurrents. Ohmic contacts allow for carrier replenished so that the photo-generated carriers can experiment several transit times before recombination [10].

Enhanced SRs were not only measured in thin film silicon devices but also in CdS/CdTe solar cells. Negatives anomalous responses with absolute value |SR| ≥ 1 have been reported in n-CdS/p-CdTe solar cells

E-mail address: frubinelli@santafe-conicet.gov.ar.

http://dx.doi.org/10.1016/j.tsf.2016.10.038
0040-6090/© 2016 Elsevier B.V. All rights reserved.

subjected to forward voltages near the open circuit voltage (V_{OC}), an scenario that can be considered as transition between the photovoltaic and photoconductive modes [11,12].

In 1995, S·Bae et al., using the computer code AMPS, predicted the so called Complementary Photo-Gating Effect (CPGE) in the blue wavelength region of the probe beam for back loaded a-Si:H/a-SiGe:H p-i-n heterojunction structures illuminated with an auxiliary DC red bias light [6]. P·Chaterjee, also obtained with computer simulations SR ≥ 1 at short wavelengths of the probe beam in a-Si:H Schottky barrier structures under red bias light illumination [7]. In both cases the presence of a highly defective front interface layer was needed to obtain SR ≥ 1. Table 1 contains a list of publications where SR ≥ 1 were reported. Some device characteristics, bias light and probe beam fluxes, and SR maximums with their corresponding wavelengths were included.

To my knowledge, the CPGE has not been yet discussed in μc-Si:H based devices. The low mobility gap of μc-Si:H makes this material an interesting candidate for the observation of the CPGE. In this paper, the conditions required to observe the CPGE in μc-Si:H devices are explored with computer simulations. The paper is organized as follows: in Section 2 the device under study and the followed methodology to calibrate our computer code are briefly described; in Section 3 the physics behind the origin of the CPGE is discussed; in Section 4 the electrical properties of the p- and p/i buffer layers

Table 1

Spectral responses greater than unity published in literature. The first column contains the reference number given the article in this contribution. The meaning of the symbols is: in column 2, W(i) = layer thicknesses of intrinsic layers, DB = defect density and σ_{DB} = capture cross sections at defect states in the intrinsic layers; N/A stands for Non-available; in columns 6 and 7, the maximum response QE_{MAX} (the absolute value $|QE_{MAX}|$ is given) and the corresponding wavelength are given or some interval when the maximum is not clearly defined; and in the last column, E (experimental data), S (simulations), BBL (Blue Bias Light), RBL (Red Bias Light), PP (Primary Photocurrent), and SP (Secondary Photocurrent). Simulations results are included only when no experimental information is available.

Ref	Device structure	Probe beam intensity (photons/cm²/s)	Bias light intensity (photons/cm²/s)	Bias light wavelength (nm)	$\|QE_{MAX}\|$	QE wavelength (nm)	Experiment simulation
[1]	a-Si:H m-i-n Schottky W(i) = 400 nm 400 hs AM1.5 Light soaked, V = 0	10^{13}–10^{14}	Variable	~436	1.06	~550	E BBL-PP
[3]	a-Si:H p-i-n light soaked W(i) = 400 nm DB = 2.4 × 10^{16} cm^{-3}, V = 0	10^{15}	6 × 10^{15}	~460	1.65	~650–690	S E confirmed BBL-PP
[4]	a-Si:H Schottky - initial state W(i) = 3000 nm DB = 2.4 × 10^{16} cm^{-3}, −V = 0.2 V	6 × 10^{13}–2 × 10^{14}	8 × 10^{15}	~400	1.75	~640–660	E S BBL-PP
[5]	a-Si:H p-i-n W(i) = 3400 nm DB = 0.5-1 × 10^{16} cm^{-3},V = −5 V, −25 V	7.4 × 10^{11}	1.5 × 10^{15}	~450	~44–46	~580–630	E S BBL-PP
[6]	Front-loaded/a-SiGe:H/a-Si:H p-i-n heterostructures, V = 0 W(i) = 50 nm/50 nm DB = 10^{17} cm^{-3}/2 × 10^{16} cm^{-3}	10^{14}	3-5 × 10^{15}	≤460	1.2–1.28	~530–580	S BBL-PP
[6]	Back-loaded a-Si:H/a-SiGe:H p-i-n heterostructures, V = 0 W(i) = 50 nm/50 nm DB = 2 × 10^{16} cm^{-3}/ 5 × 10^{15} cm^{-3} 4 × 10^{18} cm^{-3}–10 nm front layer σ_{DB} = 10^{-14} cm²/10^{-15} cm²	10^{14}	7–9 × 10^{15}	≥660	1.2–1.35	~400–430	S RBL-PP
[7]	a-Si:H Pd-i-n Schottky W(i) = 1000 nm DB = 10^{15} cm^{-3}, V = 0 10^{18} cm^{-3}–100 nm front layer σ_{DB} = 10^{-14} cm²/10^{-16} cm²	10^{14}	10^{16}	≥600	1.1	~420–440	S RBL-PP
[8]	μc-Si:H n-i-p W(i) = 1300 nm DB = 0.5–20 × 10^{15} cm^{-3}, V = 0 V	3 × 10^{13}(600 nm)	4 × 10^{16}	~380–520	1.63	~700	S E BBL-PP
[9]	a-Si:H and μc-Si:H p-i-n W(i) = 4000 nm V = −20 V	10^{13}	5.1 × 10^{16}	470	50	~580–630	S E BBL-PP
[10]	n-CdS/p-CdTe 100 nm CdS/4000 nm CdTe V = 0.80 V	1 × 10^{15}	No bias light	–	2.8	~400	S E SP
[11]	n-CdS/p-CdTe 200 nm CdS/0.2-1 × 10^4 nm CdTe V = 0.80 V	N/A	N/A	N/A	9–9.5	~300–520	S SP
[12]	a-Si:H Ni-i-n Schottky W(i) = 3000 nm initial state – V = 0.6 V	6 × 10^{13}–2 × 10^{14}	8 × 10^{15}	≤420	240	~660–680	E S BBL-SP
[12]	a-Si:H Ni-i-n Schottky W(i) = 3000 nm initial state – V = 0.6 V	6 × 10^{13}–2 × 10^{14}	5 × 10^{15}	~620	200	~660–680	E S RBL-SP
[12]	a-Si:H Ni-i-n Schottky W(i) = 3000 nm initial state – V = 0.6 V	6 × 10^{13}-2 × 10^{14}	No bias light	–	25	~660–680	E S SP

that are needed to predict the CPGE in μc-Si:H n-i-p structures are investigated in conjunction with the sensitivity of the SR to some key electrical parameters. In particular the impact of the density of defects, mobility gap, effective density of states, and free carrier mobilities of the buffer layer, the activation energy of the p-layer and the spectral content of the red bias light are explored.

2. Methodology

The device under analysis is the n-i-p device already studied by Li et al. in a previous contribution [8]. The full structure is as follows: substrate/rough Ag/ZnO back reflector/n-type nc-Si:H/intrinsic nc-Si:H/buffer/p-type nc-Si:H/ITO/Au (gridlines), with an active cell area of 0.13 cm^2. The ITO coating is 80 nm thick, while the p- and n- layers are 20 nm and 27 nm thick respectively and the light absorber intrinsic layer is ~1.3 μm thick. All silicon layers were deposited in the multi-chamber UHV system of Utrecht University called PASTA. Intrinsic layers were deposited by the Hot-Wire CVD technique using two 0.5 mm tantalum (Ta) filaments. The filament temperature was of around 1850 °C, which results in a substrate temperature of 250 °C. The $R_H = H_2 / (H_2 + SiH_4)$ gas flow ratio used was fixed to 0.952. Doped layers (p- and n-type silicon) were deposited by plasma enhanced CVD in separated chambers. The substrates were either conformal Ag/ZnO-coated Asahi U-type TCO glass, or Ag deposited at high temperatures (for proper roughness) with a ZnO coating grown by sputtering. More information can be found elsewhere [8].

The spectral response setup allowed for simultaneous application of bias light and bias voltage. The light source used to produce the bias light and the monochromatic light was a Xenon lamp. The red bias light was obtained by filtering the bias light with the long pass filter RG630, transparent for light with wavelength > 630 nm. The integrated photon flux of the bias light beam was around 7×10^{16} photons.cm^{-2} s^{-1}. The bandwidth of the monochromator was estimated as ~10 nm. Current density-voltage (J-V) characteristics were measured with a dual-beam solar simulator (WACOM) while the cells were kept at 25 °C. The optical parameters were obtained from measured reflection and transmission spectra on μc-Si:H films. The global density of states and the Urbach slope were extracted with the Dual Beam Photoconductivity technique. Other electrical input parameters were conveniently adjusted to reproduce the J-V and SR experimental data.

Our simulations were performed with the computer code D-AMPS (Analysis of Microelectronic and Photonic Devices) that solves the system of three non-linear equations (Poisson's equation and continuity equations for free electrons and holes) with the finite differences method and the Newton-Raphson method. The independent variables are the electron potential and the quasi-Fermi levels. D-AMPS is an updated version of the well-known software AMPS released by the Pennsylvania State University that includes extra features like amphoteric states, the Defect Pool-model, the Pool-Frenkel effect, a simplified treatment of light scattering, etc. [13].

The defect density was assumed uniform inside of each device layer. Defect states are represented by three pairs of Gaussian distributions, referred to as D^-, D^0 and D^+. Each pair contain donor-like states and acceptor-like states separated by the correlation energy, U, assumed equal to 0.2 eV [14]. Tail states are modelled as two exponential distributions: one with acceptor-like states connected to the conduction band and the other with donor-like states connected to the valence band. The density of states at E_C and E_V, referred to as G_{AO} and G_{DO} was assumed to be 2×10^{20} cm^{-3} eV^{-1}. Doping densities in the p- and n-layers were adjusted to reproduce the experimental activation energies. In the optical model the intensity I of the incident light is shared among N sub-beams with intensity I/N that impinge rough surfaces at different angles. The total generation rate $G(x)$ of electron-hole (e–h) pairs is obtained by summing the e-h pairs generated by each sub-beam.

Fig. 1a and b show our fittings of the light J-V characteristic measured at room temperature and AM1.5 illumination and the SR

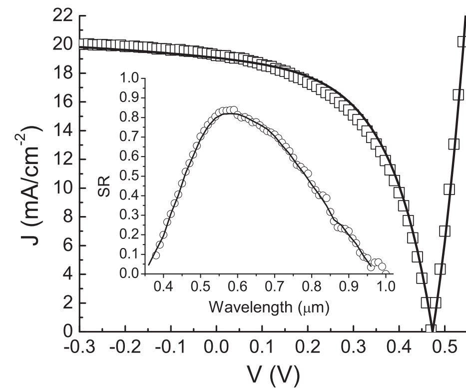

Fig. 1. Fittings (solid lines) of experimental (empty symbols) light J-V and SR characteristics. The light J-V was measured under AM1.5 illumination (squares) and the SR characteristics under red bias light illumination and at short circuit conditions (circles). The device is a μc-Si:H based n-i-p with a 1300 nm thick intrinsic layer.

measured under red bias light illumination of the μc-Si:H n-i-p device. The full list of electrical parameters adopted at the intrinsic and doped layers are listed in Table 2. The density of defects at a thin back region of the intrinsic layer next to the i/n interface was assumed higher than in the bulk (~10^{17} cm^{-3} in ~180 nm) to account for the presence of an incubation layer with a transition from the amorphous to the crystalline regime where crystallinity is evolving [15]. The SR can be matched by either including or not the incubation layer but the FF and V_{OC} of the light J-V could not be replicated well when the incubation layer was ignored. The replication of the J-V and SR curves with computer simulations were not included in our previous contribution [8] where our efforts were addressed just to reproduce experimental trends and understand the origin of the anomalous responses [8]. In this paper some electrical parameters were slightly adjusted in order to match the experimental output device characteristic curves.

3. Origin of the photogating effect under red bias light

The equations derived in this section are valid for any type of bias light and probe beam wavelengths. In SR measurements performed under bias light the sample is illuminated with two sources: the steady auxiliary bias light and the a.c. chopped monochromatic probe beam. Their flux densities are $\Phi_{BL}(\lambda)$ and $\Phi_{ML}(\lambda)$ respectively. The a.c. current component $\Delta J(\lambda)$ is synchronously detected by a lock-in amplifier. The SR characteristic under bias light is given by:

$$SR(\lambda) = \left(\frac{\Delta J(\lambda)}{q\Phi_{ML}(\lambda)}\right) = \left(\frac{J_{BL+ML}(\lambda) - J_{BL}(\lambda)}{q\Phi_{ML}(\lambda)}\right) \quad (1)$$

where q is the electron charge, λ is the wavelength, $J_{BL+ML}(\lambda)$ is the current density obtained when the sample is simultaneously illuminated with the bias light (BL) and the probe beam (ML), and J_{BL} is the current density obtained when the sample is illuminated with only the bias light.

Combining the continuity equation for holes and taking into account that the electrical current is given by the sum of the electron and hole components, $J_{BL}(\lambda)$ can be expressed as:

$$J_{BL}(\lambda) = \int_0^W G_{BL}(\lambda, x)dx - \int_0^W R_{BL}(\lambda, x)dx - J_{e-BL}(\lambda, 0) - J_{h-BL}(\lambda, W) \quad (2)$$

where $G_{BL}(\lambda,x)$ and $R_{BL}(\lambda,x)$ are the generation and recombination rates under BL illumination at the x-position respectively, $J_{e\text{-}BL}(\lambda,0)$ is the electron back diffusion current at the front contact (x = 0), and $J_{h\text{-}}$

Table 2
List of electrical input parameters used in our J-V and SR fittings. The meaning of the symbols is as follows: W layer thickness, E_G mobility gap, N_c and N_v effective density of states in the conduction and valence band respectively, G_{AO} and G_{DO} are the density of states at the conduction and valence band edges respectively, N_A and N_D acceptor and donor doping densities in the p- and n-layers, μ_N and μ_P electron and hole mobilities, E_D and E_A valence and the conduction tail slopes, t_N and t_P capture cross section for electrons and holes at tail states, D^-, D^0 and D^+ densities of defect states enclosed in the three Gaussians, E^-, E^0 and E^+ peak positions of the Gaussians, s_D standard deviations, σ_N and σ_P capture cross sections for electrons an hole at defect states, U correlation energy, E_{ACT} activation energy. The superscripts +, 0 and – indicate the charge state of defect states. The right column contains the parameters of a (p)-a-SiC:H layer used to explore the CPGE.

Parameters	p-μc-Si:H	buffer-a-Si:H	i-μc-Si:H	n-μc-Si:H	p-a-SiC:H
W (nm)	20	5	1300	27	20
$\mathbf{E_G}$ (eV)	1.2	2	1.25	1.2	2
$\mathbf{N_c}, \mathbf{N_v}$ (cm^{-3})	3×10^{19}	2×10^{20}	6×10^{19}	3×10^{19}	2×10^{20}
$\mathbf{G_{AO}}, \mathbf{G_{DO}}$ (cm^{-3})	2×10^{20}	10^{21}	2×10^{20}	2×10^{20}	10^{21}
μ_N (cm^2 V^{-1} s^{-1})	40	20	25	40	10
μ_P (cm^2 V^{-1} s^{-1})	4	2	10	4	1
$\mathbf{E_D}$ (meV)	30	48	35	30	80
$\mathbf{E_A}$ (meV)	25	30	23	25	45
$\mathbf{t_N^+}$ $\mathbf{t_P^-}$ (cm^2)	5×10^{-15}	1×10^{-15}	1×10^{-15}	5×10^{-15}	1×10^{-15}
$\mathbf{t_N^0}$ $\mathbf{t_P^0}$ (cm^2)	5×10^{-17}	1×10^{-17}	1×10^{-17}	5×10^{-17}	1×10^{-17}
$\mathbf{D^-}$ (cm^{-3})	2×10^{18}	3×10^{15}	5.8×10^{15}	2×10^{18}	2.0×10^{18}
$\mathbf{D^0}$ (cm^{-3})	1×10^{18}	1.5×10^{15}	2.9×10^{15}	1×10^{18}	1×10^{18}
$\mathbf{D^+}$ (cm^{-3})	2×10^{18}	3×10^{15}	5.8×10^{15}	2×10^{18}	2.0×10^{18}
$\mathbf{E_{D^-}}$ (eV)	0.235	0.67	0.27	0.235	0.9
$\mathbf{E_D^0}$ (eV)	0.535	0.97	0.57	0.535	1.2
$\mathbf{E_D^+}$ (eV)	0.835	1.27	0.87	0.835	1.5
$\mathbf{s_D}$ (eV)	0.1	0.13	0.1	0.1	0.13
U (eV)	0.2	0.2	0.2	0.2	0.2
$\boldsymbol{\sigma_N^+}$ $\boldsymbol{\sigma_P^-}$ (cm^2)	5×10^{-14}	1×10^{-15}	10^{-15}	5×10^{-14}	5×10^{-15}
$\boldsymbol{\sigma_N^0}$ $\boldsymbol{\sigma_P^0}$ (cm^2)	5×10^{-15}	1×10^{-16}	10^{-17}	5×10^{-15}	5×10^{-16}
$\mathbf{N_A{-}N_D}$ (cm^{-3})	9.5×10^{18}	–	–	1.53×10^{19}	5.15×10^{18}
$\mathbf{E_{ACT}}$ (eV)	0.059	0.95	0.58	0.025	0.47

$_{BL}(\lambda,W)$ is the hole back current at the back contact ($x = W$) all specified at the wavelength λ. Following a similar reasoning the current $\Delta J(\lambda)$ of Eq. (1) can be expressed as:

$$J_{BL+ML}(\lambda)-J_{BL}(\lambda) = \int_0^W G_{ML}(\lambda,x)dx - \int_0^W [R_{BL+ML}(\lambda,x)-R_{BL}(\lambda,x)]dx - [J_{e-BL+ML}(\lambda,0)-J_{e-BL}(\lambda,0)] - [J_{h-BL+ML}(\lambda,W)-J_{h-BL}(\lambda,W)] \quad (3)$$

In Eq. (3) the currents associated to the generation rate $G_{BL}(x)$ cancel in the subtraction. The Optical Spectral Response $SR_{OPT}(\lambda)$ can be defined as:

$$SR_{OPT}(\lambda) = \frac{\int_0^W G_{ML}(x,\lambda)dx}{q\Phi_{ML}(\lambda)} \leq 1$$

Optical losses, like reflection at the front contact and incomplete absorption of light, maintain $SR_{OPT}(\lambda)$ below unity. As the hole back diffusion current at the back contact is negligible in μc-Si:H n-i-p devices Eq. (1) can be expressed as:

$$SR(\lambda) \cong SR_{OPT}(\lambda) + \frac{\int_0^W [R_{BL}(\lambda,x)-R_{BL+ML}(\lambda,x)]dx + [J_{e-BL}(\lambda,0)-J_{e-BL+ML}(\lambda,0)]}{q\Phi_{ML}(\lambda)} \quad (4)$$

Hence, spectral responses above unity are only possible when the electrical losses taking place in the device under bias light illumination are higher than their counterparts under simultaneous bias and monochromatic light illumination. In optimized μc-Si:H devices the electron back diffusion current at the front contact is lower than the total recombination loss taken place in the active layers. So Eq. (4) can be approximated as:

$$SR(\lambda) \cong SR_{OPT}(\lambda) + \frac{\int_{p-layer} [R_{BL}(\lambda,x)-R_{BL+ML}(\lambda,x)]dx + \int_{buffer-layer} [R_{BL}(\lambda,x)-R_{BL+ML}(\lambda,x)]dx}{q\Phi_{ML}(\lambda)} \quad (5)$$
$$\frac{\int_{i-layer} [R_{BL}(\lambda,x)-R_{BL+ML}(\lambda,x)]dx + \int_{n-layer} [R_{BL}(\lambda,x)-R_{BL+ML}(\lambda,x)]dx}{q\Phi_{ML}(\lambda)}$$

SR measurements in solar cells are performed under either bias light illumination or in the absence of bias light; i.e. under dark conditions. In the first case the bias light is usually AM1.5, which is a polychromatic source. In this case the incident bias light flux $\Phi_{BL}(\lambda)$ and the monochromatic flux $\Phi_{ML}(\lambda)$ fulfill the following condition: $\Phi_{BL}(\lambda) \gg \Phi_{ML}(\lambda)$ at every wavelength λ. Electron-hole pairs generated by the probe beam are not able to significantly alter the electric field profile already tailored by trapping of free carrier photo-generated by the bias light. In this scenario, and also under dark condition, the SR is always below unity. In order to obtain SRs higher than one the relationship $\Phi_{BL}(\lambda) \gg \Phi_{ML}(\lambda)$ should not be fulfilled at least inside of some region of the device. Hence, the probe beam and the auxiliary bias light should have different spectral distributions.

4. Results

As the CPGE will be discussed in this contribution the DC red bias light and the AC blue probe beam will be recognized as RBL (Red Bias Light) and BML (Blue Monochromatic Light) respectively.

Using the parameters of Table 2 the recombination losses in each layer and the back-electron diffusion at the front contact followed the usual relationships $R_{RBL} \leq R_{RBL+BML}$ and $J_{n\text{-}RBL} \leq J_{n\text{-}RBL+BML}$ respectively. In the contributions of Bae et al. and Chaterjee [6,7] SR > 1 were predicted at short wavelengths in devices under RBL illumination when a highly defective layer was included at the front region of the device. Taking

into account their results the electrical parameters of the p/i buffer layer were modified: the density of defects was increased by several orders, the thickness was also increased, the mobility gap was lowered in successive steps, and free carrier mobilities and capture cross sections were modified. However none of these modifications gave rise to SR > 1. Fig. 2 shows the band diagram obtained with D-AMPS of the n-i-p solar cell at short circuit conditions and under RBL illumination (filter RG630). In order to make the a-Si:H buffer layer more visible, its thickness was increased to 20 nm.

4.1. Defective buffer layer and a-SiC:H p-layer

In order to explore alternative scenarios where SR could be over unity, the (p)-μc-Si:H layer was replaced by its counterpart of (p)-a-SiC:H with the characteristic deposition conditions used at Utrecht University and reported in previous collaborations [16]. The electrical parameters of the (p)-a-SiC:H layer are listed in Table 2 [16]. The wide-gap (p)-a-SiC:H layer (2.0 eV) significantly reduces the recombination losses at the front-p-layer and the electron back diffusion at the front contact making SR more sensitive to recombination losses taking place inside the intrinsic layer.

4.1.1. Sensitivity of SR > 1 to electrical parameters of the defective buffer layer

In the alternative μc-Si:H n-i-p device with the (p)-a-SiC:H the electrical parameters of the p/i buffer layer such as the mobility gap, density of DBs, and thickness, were again modified. This time our code was able to predict anomalous responses above unity when the buffer layer at the p/i interface was assumed to be quite defective. In order to obtain SR > 1 the defective buffer layer (see parameters listed in Table 3) should approximately have a defect density between 6.8×10^{17} cm^{-3} and 2.2×10^{18} cm^{-3}, a mobility gap wider than 1.55 eV and narrower than 2.23 eV, and a thickness between 16 nm and 40 nm. Outside of the window defined by these three electrical parameters SR_{MAX} remains below unity. Of course, the CPGE disappears when the defective layer is removed. The CPGE is also a function of the hole and electron mobilities, trap capture cross sections, and defect energies assumed for the defective buffer layer. In all cases SR_{MAX} was predicted at short wavelengths to be higher than the values obtained by Bae et al. in a-Si:H/a-SiGe:H p-i-n heterojunction devices [6] and by Chaterjee in a-Si:H Schottky barriers [7]. For instance SR_{MAX} ~1.66 was predicted at ~500 nm for a 20 nm thick buffer layer, with a 1.65 eV mobility gap, and a defect density of 10^{18} cm^{-3}. Table 3 compares the electrical parameters of this defective buffer layer (DBUL) with the ones of the regular buffer layer (RBUL) used to match the J-V and SR of Fig. 1. The right column of Table 3 shows the predicted SR peaks and the corresponding wavelengths when only one of the electrical parameters of the DBUL is replaced by its counterpart of the RBUL. Table 3 demonstrates that the key electrical parameters to obtain the CPGE are the three already

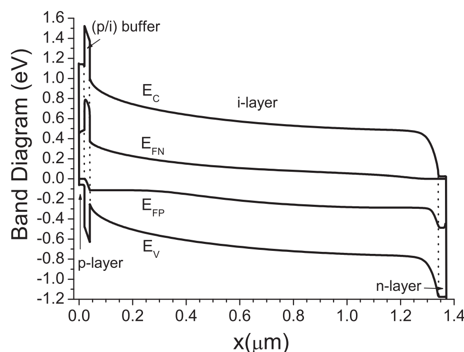

Fig. 2. Band diagram of the μc-Si:H n-i-p solar cell at short circuit conditions and under red bias illumination. The a-Si:H buffer layer thickness was assumed 20 nm.

Table 3
Comparison between the electrical parameters of the p/i defective buffer layer used to predict the CPGE (left column) and the regular buffer used to match the J-V and SR characteristics of the (p)-μc-Si:H/buffer/(i)-μc-Si:H/(n)-μc-Si:H structure (middle column). The right column shows the predicted SR peak and its wavelength when only one parameter of the defective buffer is replaced by its counterpart of the regular buffer layer. The defect densities (D^-, D^0, D^+) in the three Gaussian distributions were simultaneously changed.

Parameters	Reference Defective buffer	Regular buffer	1.661–500 SR_{MAX}-λ_{MAX}(nm)
W (nm)	20	5	0.818–560
$\mathbf{E_G}$ (eV)	1.65	2	2.220–460
Nc (cm^{-3})	8×10^{19}	2×10^{20}	1.611–500
Nv (cm^{-3})	8×10^{19}	2×10^{20}	1.372–500
μ_N ($cm^2\ V^{-1}\ s^{-1}$)	10	20	1.446–500
μ_P ($cm^2\ V^{-1}\ s^{-1}$)	1	2	1.510–500
$\mathbf{D^-}$ (cm^{-3})	4×10^{17}	3×10^{15}	0.816–580
$\mathbf{D^0}$ (cm^{-3})	2×10^{17}	1.5×10^{15}	0.816–580
$\mathbf{D^+}$ (cm^{-3})	4×10^{17}	3×10^{15}	0.816–580
σ_N^+ (cm^2)	7.5×10^{-15}	1×10^{-15}	1.072–460
σ_P^0 (cm^2)	7.5×10^{-17}	1×10^{-16}	1.592–500
σ_P^- (cm^2)	7.5×10^{-15}	1×10^{-15}	1.619–460
σ_N^0 (cm^2)	7.5×10^{-17}	1×10^{-16}	1.661–500

mentioned (density of defects, thickness, and mobility gap) plus the capture cross sections for electrons at donor-like states and the effective density at the valence band. Table 3 also indicates that the SR is sensitive to free carrier mobilities. Detailed simulations, not included here, indicate no sensitivity to tail states: either to their density or capture cross sections.

Our simulations show that the RBL introduces a redistribution of the electric field existing at thermodynamic equilibrium conditions. The electric field becomes reinforced near the interfaces and weakened in the bulk by the RBL. Two effects are competing:

(a.) in the bulk electrons and holes photo-generated by the RBL are more easily trapped by positively and negatively charged donor and acceptor states respectively rather than by neutral defect states due to coulombic attraction. Electron and hole concentrations are comparable; and

(b.) free carriers photo-generated by the RBL and not trapped by defect states are drifted by the electric field along the intrinsic layer increasing the concentration of majority free carriers near the interfaces with respect to their counterparts at equilibrium. As trapping is determined more by majority than by minority carriers, near the interfaces charged traps with the opposite charge than free carriers are found in lower concentrations than in the bulk becoming trapping by neutral defect states more significant. Hence, the RBL increases the positive (negative) trapped charge density near the p/i (i/n) interface and decreases the positive and negative charge densities in the intrinsic layer bulk.

The origin of the CPGE can be basically understood by comparing the charge density, electric field, and recombination profiles when both lights, BML and RBL, are simultaneously impinging at the front contact of the sample and when only the RBL is illuminating the sample. Fig. 3a, b, and c show these profiles in the (p)-a-SiC:H layer, the defective buffer, and the intrinsic layer. In order to simplify the discussion the incubation layer next to the i/n interface was not included in Fig. 3. The incubation layer just provides some additional recombination losses but the physics behind the CPGE is the same. In Fig. 3 the intensity of the probe beam was assumed conveniently higher than in experiments to facilitate the visualization of the differences existing under both illumination conditions. The a.c. BML, which is strongly absorbed at the front region of the device, modulates the positive charge trapped at the numerous defects present in the defective layer. The density of trapped

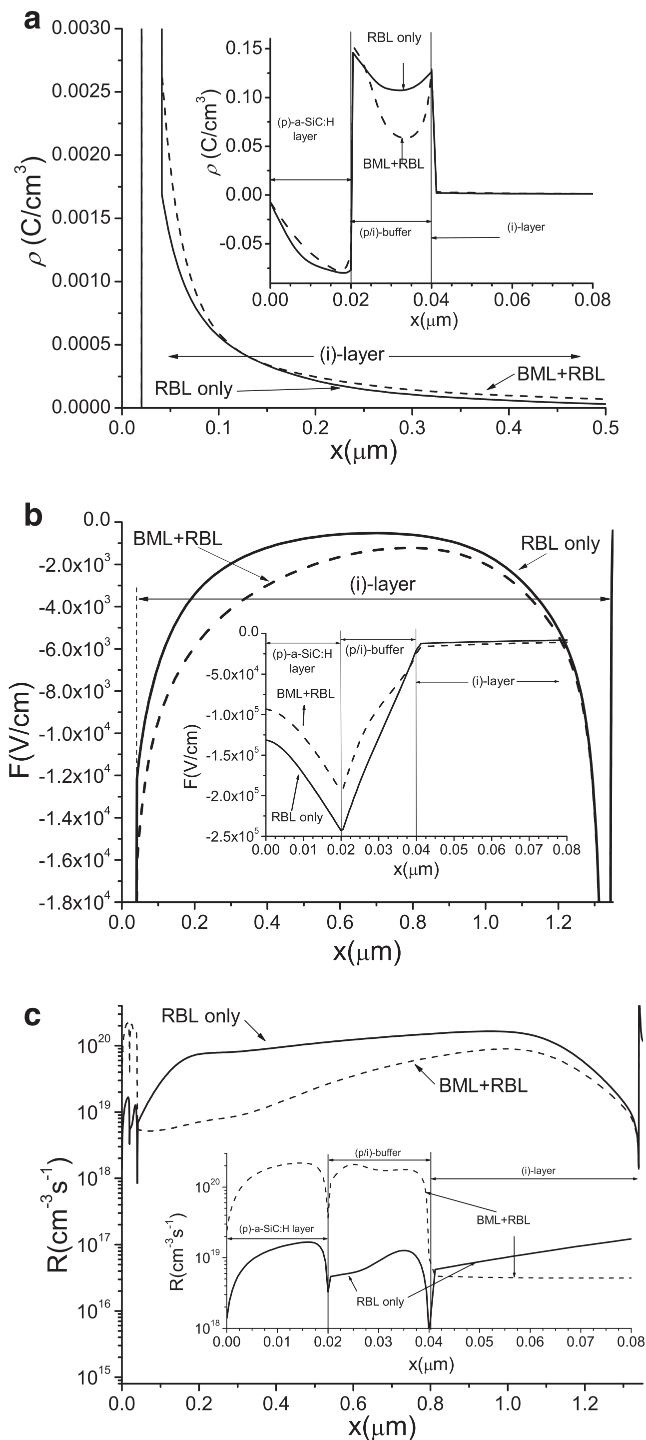

Fig. 3. (a) Charge density, (b) electrical field, and (c) recombination rate profiles in the μc-Si based n-i-p junction with a 1300 nm thick intrinsic layer when only the RBL (solid line) and when both the RBL and BML (dash line) are impinging on the front contact. The optical filter cut-off wavelength was adopted as 710 nm. Insets show a magnified view at the front device regions. The incubation layer next to the back i/n interface was not included.

holes at donor-like tail states at the defective buffer layer is negligible in comparison with its counterpart at defect states (DBUL) under any illumination condition. The incident BML superimposed to the RBL lowers the net positive charge trapped at the defective layer when only the RBL is on (Fig. 3a). A similar but less intense modulation of the positive trapped charge can be observed inside the p-layer (Fig. 3a). Hence, the BML generates an electrical dipole with a positive charge trapped at the buffer layer and a net negative charge (ionized acceptors minus trapped charge in donor-like defect states) at the (p)-a-SiC:H layer that is pulsing at the frequency of the optical chopper. The BML generates a considerable number of e-h pairs near the front contact where the a.c. dipole is located. The predominance of positively charge at donor-like localized states in front layers favors trapping of electrons photo-generated by the BML due to Coulombic attraction. A considerable fraction of holes photo-generated by the BML exit the device without getting trapped due to its proximity to the front contact while electrons drifted by the electric field in the opposite direction are trapped along the whole device and in particular a significant fraction at the defective layer. The reduction of the positive charge hosted in the defective layer lowers the electric field intensity inside the two front layers. As the integral of the electric field profile must remain constant along the whole device the electric field should become strengthen inside the intrinsic layer (see Fig. 3b). In this scenario a smaller portion of electrons and holes photo-generated by both the BML and RBL become trapped at defect states. Hence the positive and negative charge densities of trapped carriers in the intrinsic layer increase with respect to their counterparts under RBL illumination. Interestingly this increase in the bulk of trapped charge densities under RBL illumination is another signature of the CPGE which is the opposite effect observed when $SR < 1$ where densities of trapped carriers are lower than at equilibrium under either RBL or simultaneous RBL + BML illumination. The BML beam is able to modulate the electric field in the whole device: the field is reinforced inside the intrinsic layer and weakened in the front layers. This effect gives rise to the modulation of the recombination rate that becomes lower inside the intrinsic layer under simultaneous RBL + BML illumination than under only RBL illumination. Fig. 3c shows that the condition $R_{RBL} \geq R_{RBL\ +\ BML}$ is clearly fulfilled in the low μc-Si:H mobility gap intrinsic layer where recombination losses are significant. The charge redistribution taking place in the back region of the intrinsic layer is not very significant because most of electrons generated by the BML are already trapped or recombine before reaching the i/n interface. The increase of the positive charge at the front region of the intrinsic layer by the BML illumination is not significant in comparison with the decrease of the positive charge taken place at the defective layer which is the responsible for the electric field redistribution inside the intrinsic layer. The modification of the recombination rate profile introduced by the BML clearly indicates that $SR > 1$ at short wavelengths is caused by the modulation of the recombination rate inside the intrinsic layer and not in the doped and defective buffer layers (Fig. 3c). Since the wavelength of the probe beam is short the recombination loss in the intrinsic layer is more significant near the p/i interface than in the bulk. On the other hand, the modulation of the electric field is originated by the modulation of the positive charge trapped in the defective buffer layer tailored by the capture of electrons generated by the BML.

Fig. 4a shows SR as function of the mobility gap of the defective layer. The highest SR_{MAX} is obtained for a mobility gap of ~1.85 eV (~2.54 at 460 nm). Higher or lower mobility gaps can host less positive trapped charge in the buffer layer. In defective layers with lower gaps trapped holes are more easily emitted to extended states because defect states are located closer to the valence band edge. In defective layers with higher mobility gaps the energy offset at the valence band edge of the buffer/intrinsic interface would hinder trapping of holes at the buffer layer that were photo-generated inside the intrinsic layer. Hence in both cases electrons generated by the BML will have a lower concentration of trapped positive charge available for modulation inside the defective layer.

Fig. 4b shows the SR as function of the density of defects in the defective layer. Similar trends are obtained with respect to the defective layer thickness because SR_{MAX} is actually function of the product between the density of defects and the buffer layer thickness; i.e. of the total number of defects present in the defective layer. Adopting a density of defects of 10^{18} cm^{-3} the enhancement of the SR at ~500 nm is already observed for a 12 nm thick buffer layer but the SR overcomes unity for buffer layers thicker than 15 nm. The thickness of the defective layer was

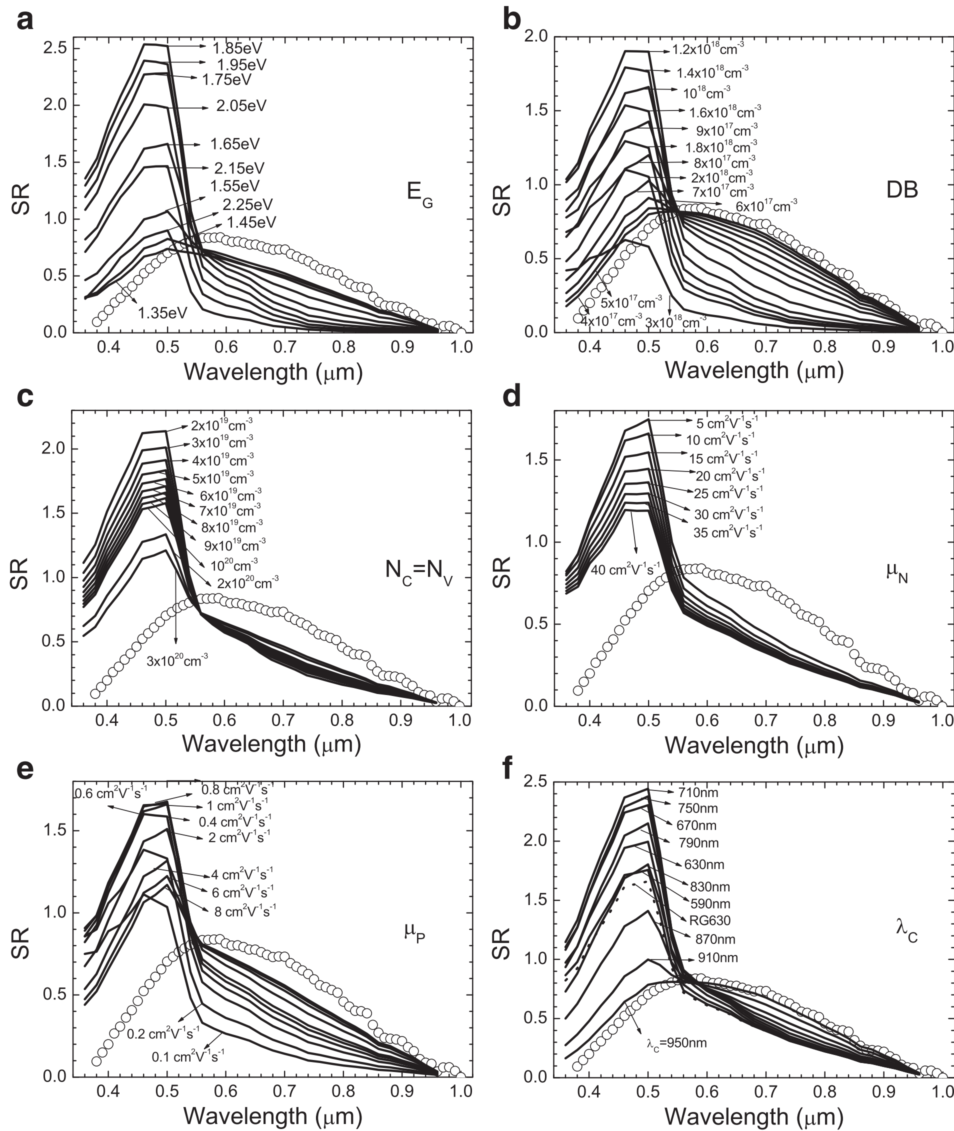

Fig. 4. SR at short circuit conditions of the μc-Si:H based n-i-p device illuminated with a RBL as function of the: (a) p/i buffer layer mobility gap, (b) density of defects at the defective buffer layer, (c) effective density of states at the conduction and valence bands, (d) electron mobility, (e) hole mobility and (f) the cut-off wavelength λ_c of an ideal optical long-pass filter. Parameters of the defective buffer layer can be found in the left column of Table 3. Dots correspond to the SR obtained with the filter RG630. The experimental SR matched with the parameters of Table 2 is included for comparison purposes.

selected in Fig. 4a as 20 nm. When either the density of defects or(and) the thickness of the defective layer is small the positive charge trapped at donor-like defect states modulated by the BML is not enough to significantly alter the electric field inside the intrinsic layer. In the other extreme, when the density of defects is very high and/or the defective layer is very thick, the modulated positive charge trapped at defect states of the buffer layer would overcome at certain point the net negative charge of the ionized doping atoms hosted by the (p)-layer. Hence a significant band bending at the (p)-layer is created to generate more negative charge that could compensate the excessive positive charge trapped present at the defective layer to reach the charge neutrality condition. The strong dipole created at the front layers of the device collapses the electric field inside the intrinsic layer making recombination losses so significant that the current collected under BML becomes much lower and the SR very poor and below unity.

The CPGE is sensitive to capture cross sections of donor-like defect states while it is insensitive to capture cross sections of acceptor-like defect states (see Table 3). This result can be easily explained by the proximity of the defective layer to the p-layer where holes are majority carriers. The trapped carrier concentration is dominated by the (positive) charge hosted at donor-like states, while the (negative) charge trapped at acceptor-like states is much lower. Lower values of SR_{MAX} are obtained when either σ_P^0 is increased, σ_N^+ is decreased, or N_V is increased. Our simulations indicate that in these cases a higher concentration of positive charge is trapped at donor-like defect states of the buffer layer under RBL illumination that weakens the electric field inside the intrinsic layer. Hence the BML modulates a less intense field in the intrinsic layer and consequently differences between the recombination losses under RBL + BML and RBL illumination become less significant. The dependence of SR_{MAX} with respect to σ_P^0, σ_N^+, and N_V are monotonically increasing functions. The CPGE is lost for capture cross sections such us $\sigma_N^+ < \sim 7.5 \times 10^{-16}$ cm^2 and $\sigma_P^0 > \sim 7 \times 10^{-16}$ cm^2, while SR_{MAX} remains above one for any N_V within the range reported in literature for a-Si:H and μc-Si:H [16–18]. Fig. 4c shows SR as function of the effective densities of states adopted in the defective buffer layer.

Our sensitivity studies indicate that the SR is also function of the electron and hole mobilities adopted at the defective layer [21–24].

SR_{MAX} is a monotonically decreasing function of μ_N while it shows a maximum at μ_P ~ 0.6–0.8 $cm^2 V^{-1} s^{-1}$. The CPGE is preserved for any reasonable value of μ_N and μ_P reported for a-Si:H or μc-Si:H (CPGE is lost when $\mu_P < 0.08$ $cm^2 V^{-1} s^{-1}$) [21–24]. Figs. 4d and e illustrate these results. Different free carrier mobilities impact in the predicted SR_{MAX} by altering the concentration of positive charge trapped accumulated at donor-like defect states. With respect to the electrical parameters of the (p)-a-SiC:H layer the SR is sensitive to the hole mobility showing a similar trend to the one obtained at the defective layer.

4.1.2. Sensitivity of SR > 1 to electrical parameters of the intrinsic layer

As the BML is mainly absorbed at the front region of the device the SR is more sensitive to electrical parameters of defects states located at the front region of the intrinsic layer. The SR shows lower and lower sensitivity to defect states located further and further from the p/i interface as long as the density of defects in the intrinsic layer bulk is uniform. The transition from high to low dependence is gradual. However in our device, the incubation layer next to the i/n interface with a higher density of defects could make a no negligible contribution to the CPGE. For instance with the parameters of Table 2 and the defective buffer layer described in Table 3 when the 180 nm thick incubation layer with a defect density of 2.5×10^{17} cm^{-3} is removed SR_{MAX} at 500 nm drops from 1.66 to 1.49.

The dependence of SR on the electrical parameters of the intrinsic layer is slightly different when there is or there is not an incubation layer present at the back region of the intrinsic layer. When the incubation layer is absent the following trends are obtained:

(a.) SR_{MAX} becomes practically insensitive to the intrinsic layer thickness for thicker layers. SR_{MAX} increases by <1% when its thickness is increased in steps of 100 nm beyond 1800 nm. SR_{MAX} monotonically decreases for thinner intrinsic layers because the BML becomes less efficient in modulating the more robust electric field present in the intrinsic layer;

(b.) SR_{MAX} is near the maximum for the density of defects in the intrinsic layer obtained from our fittings (see Table 2). Lower defect densities are accompanied by modulation of lower recombination rates and higher defect densities tend to shield and weaken the electric field inside the intrinsic layer and consequently less photo-generated holes reach the defective layer and become trapped. Hence there is an optimum electric field intensity inside the intrinsic layer that maximizes SR_{MAX}: very strong electric fields are more difficult to be modulated by the BML and very weak fields magnify recombination losses under either RBL and RBL + BML illumination in such extend that the CPGE is lost;

(c.) SR decreases for higher mobility gaps because the BML modulates lower recombination losses inside the intrinsic layer (the CPGE is lost for $E_G > 1.4$ eV);

(d.) SR_{MAX} shows little dependence with respect to the density of defects at the mobility edge and increases for higher effective density of states at the conduction and valence band. The CPGE is not lost for any reasonable values of N_C and N_V;

(e.) SR_{MAX} shows more sensitivity to neutral than charged capture cross sections of defect states. In any case the CPGE is preserved for the capture cross sections used in literature.

(f.) SR_{MAX} declines significantly only for very low free carrier mobilities [25–27]. The needed conditions to preserve the CPGE are electron and hole mobilities in the intrinsic layer not lower than 5 $cm^2 V^{-1} s^{-1}$ and 0.4–0.5 $cm^2 V^{-1} s^{-1}$ respectively. In the other extreme of intrinsic μc-Si:H layers with high free carriers mobilities SR_{MAX} reaches saturation for $\mu_P > 8$–10 $cm^2 V^{-1} s^{-1}$ and $\mu_N > 20$ $cm^2 V^{-1} s^{-1}$ [25–27].

(g.) The CPGE is weaker in samples with μc-Si:H intrinsic layers of lower activation energies and stronger in samples with a defective layer next to the p/i interface.

Some minor differences are found in the predicted trends when the incubation layer is present in the back region of the intrinsic layer:

(a.) SR_{MAX} increases below 1% when its thickness is increased in steps of 100 nm for intrinsic layers already thicker than 1200 nm;

(b.) SR_{MAX} decreases for higher densities of defects but increases very little for lower densities of defects reaching a sort of saturation at ~1.5–2×10^{16} cm^{-3};

(c.) SR_{MAX} shows the same but less pronounced trend with respect to the density of states at the conduction and valence band;

(d.) SR_{MAX} reaches saturation for higher hole mobilties $\mu_P \geq 15$ $cm^{2}V^{-1} s^{-1}$. The CPGE is lost for low electron mobilities such as $\mu_N \leq 4$ $cm^2 V^{-1} s^{-1}$. The CPGE is weaker in samples with a defective layer at the front region of the intrinsic layer.

4.1.3. Sensitivity of SR > 1 to the spectral content of the auxiliary bias light

The CPGE is very sensitive to the spectral content of the RBL as shown in Fig. 4d. The long-pass optical filter is assumed ideal with a sharp transition at λ_C (transmittance drops from 1 to 0 at λ_C) while the RG630 filter has a gradual transition at $\lambda_C = 630$ nm. Our simulations show that SR_{MAX} grows until reaching its maximum for a cut-off wavelength of $\lambda_C = 730$ nm (not included in Fig. 4d) being $SR_{MAX}(\lambda_C = 730\ nm)$ ~ 2.46 which is only slightly higher than $SR_{MAX}(\lambda_C = 710\ nm)$ ~ 2.44. SR_{MAX} is located at 500 nm for any cut-off wavelength but the SR is higher than one for a wide region of the spectrum (roughly between 360 nm and 540 nm). An optical filter with a higher cut-off wavelength blocks the absorption of photons with lower wavelengths that are not uniformly absorbed. The asymmetry between the generation rate profiles G_{BML} and G_{RBL} created by the BML probe beam and the auxiliary light RBL respectively (see Eqs. (2) and (3)) is essential to generate SR over the unity. The modulation of the electric field by the BML becomes more efficient without the absorption of photons in the yellow, green or orange region of the spectrum. When the cut-off wavelength of the optical filter is increased further and further or/and when a band-pass filter is interposed to also limit the longest wavelength the CPGE becomes weaker due to the lower generation of e-h pairs created by the RBL.

The CPGE is also function of the RBL intensity. The highest SR_{MAX} predicted by D-AMPS was ~3.36 for a RBL light intensity of 4.5×10^{17} photons·cm^{-2} s^{-1} (~10 times higher than in our simulations) and $\lambda_C = 710$ nm. The probe beam intensity was assumed 5×10^{13} photons.$cm^{-2}s^{-1}$. SR_{MAX} decreases for higher BML intensities and finally the CPGE is lost when the intensity is increased to ~3.95×10^{15} photons·cm^{-2} s^{-1} (~80 times more than in our simulations) and only increases by 0.9% when the intensity of the probe beam is reduced to only 10^{11} photons.$cm^{-2}s^{-1}$ and saturates for lower intensities. It is important to realize that at lower intensities the profile of the electric field is less perturbed by the BML and that the SR is defined with respect to the photon flux of the probe beam $\Phi_{ML}(\lambda)$ (see Eq. (1)). Trends obtained for the CPGE are similar to the ones reported for the conventional PGE but changes in SR with respect to the bias light and probe beam intensities are less pronounced because the modulation of charge is taking place in a narrow defective layer rather than in the whole intrinsic layer. The modulation of the positive charge trapped at defect states located in the front region of the intrinsic layer does not contribute to the CPGE.

4.2. Sensitivity of SR > 1 to the activation energy of the μc-Si:H p-layer

The regular experimental activation energies of the (p)-a-SiC:H, (p)-μc-Si:H, and (n)-μc-Si:H layers grown at Utrecht University are of 0.47 eV, 0.059 eV, and 0.025 eV respectively [18,19]. Assuming that

offsets at interfaces of materials with different mobility gaps are symmetrically distributed between the conduction and valence band edges the built-in potential of the n-i-p structures with the (p)-a-SiC:H and (p)-μc-Si:H layers can be estimated as (see Table 2) 1.104 eV and 1.115 eV respectively. The built-in potential of the n-i-p structure with the (p)-a-SiC:H front layer is only slightly lower than the one with the (p)-μc-Si:H layer. However the offsets at the buffer/i layer interface are considerable higher in the n-i-p structure with the (p)-a-SiC:H. The higher activation energy of the (p)-a-SiC:H layer hinders the exit of holes at the front contact favoring trapping of holes at front layers that partially shields and deteriorates the electric field inside the intrinsic layer as discussed in a previous contribution [20]. When the (p)-μc-Si:H layer is replaced by the (p)-a-SiC:H layer the presence of the offset at the p/i interface is also crucial to create the appropriate scenario for the prediction of SR > 1; i.e. to make more efficient the modulation of charge and electric field by the BML. This is illustrated in Fig. 5 where the electron potential profiles at equilibrium and under RBL illumination are compared in both n-i-p structures for the regular (Table 2) and defective buffer layers (Table 3). Fig. 5 shows already at thermodynamic equilibrium conditions the shielding of the electric field introduced by the defective layer that becomes more pronounced under RBL illumination. SR higher than one is predicted because the effective built-in potential is considerably reduced by the RBL and enhanced back by the BML. Detailed simulations not included here indicate that when the mobility gap of the (p)-layer is lowered in successive steps SR_{MAX} decreases but the CPGE is not completely lost. The doping density was adjusted to maintain the activation energy as 0.47 eV. On the other hand when the mobility gap of the p-layer is maintained as 2.0 eV and the doping density is increased the CPGE is finally lost for activation energies near or lower than 0.3 eV, a value that is very difficult to achieve in practice. Flat band conditions were assumed at both contacts.

These results opened the possibility that n-i-p devices containing a defective buffer and a (p)-μc-Si:H layer with a lower doping concentration; i.e. with an activation energy E_{ACT}(p) higher than 0.059 eV (see Table 2) could also show the CPGE. The reduction of the effective built-in potential and the electric field intensity in the intrinsic layer in conjunction with significant trapping of free holes at the high number of donor states in the defective buffer layer might be the appropriate scenario to obtain CPGE in n-i-p devices with (p)-layers of μc-Si:H. Fig. 6 shows that the CPGE is indeed predicted for (p)-μc-Si:H layers with activation energies E_{ACT}(p) higher than ~0.13 eV (boron density $N_A < \sim 6.9 \times 10^{18}$ cm^{-3}) and lower than 0.46 eV ($N_A > \sim 2.3 \times 10^{18}$ cm^{-3}). Outside of this range the electric field in the intrinsic layer is either too strong or too weak to be efficiently modulated by the BML and the CPGE is lost. The highest SR_{MAX} ~ 1.79 is obtained for E_{ACT}(p) ~ 0.286 eV ($N_A \sim 4 \times 10^{18}$ cm^{-3}) at ~500 nm. Flat band conditions were also assumed in these simulations. The dependence of the CPGE with respect to the cutoff wavelength of the long-pass optical filter, to the mobility gap ($E_{G\text{-}BUFF}$), density of defects (DB_{BUFF}), and to the effective density of states at bands of the defective buffer layer ($N_{C\text{-}V\text{-}BUFF}$), are similar to the ones already described in Section 4.1 for a μc-Si:H n-i-p device with a (p)a-SiC:H layer. The highest SR_{MAX} predicted by D-AMPS for a (p)μc-Si:H layer with a doping density of $N_A = 4 \times 10^{18}$ cm^{-3} are: 2.05 for $E_{G\text{-}BUFF} = 1.75$ eV, 1.865 for $DB_{BUFF} = 2.3 \times 10^{18}$ cm^{-3}, 2.06 for $N_{C\text{-}V\text{-}BUFF} = 2 \times 10^{19}$ cm^{-3}, and 3.09 for $\lambda_C = 750$ nm, all at 500 nm. Electrical parameters at the defective layer were changed one at a time.

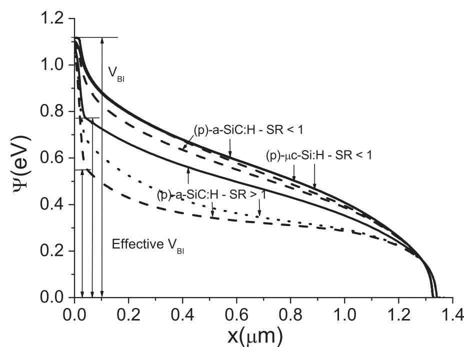

Fig. 5. Electron potential Ψ(x) at zero voltage of the μc-Si:H n-i-p structure: (a) with a (p)-μc-Si:H layer and parameters of Table 2 (Ψ(x) at thermodynamic equilibrium and under RBL illumination are practically on the top of each other); (b) with a (p)a-SiC:H layer and a good quality p/i buffer layer (SR < 1, parameters of the second column of Table 2) and with a (p)a-SiC:H layer and a defective p/i buffer layer (SR > 1, parameters of the left column of Table 3). Solid lines correspond to thermodynamic equilibrium, dash lines to illumination with the RBL, dotted line to illumination with the RBL and BML. The probe beam intensity was conveniently magnified in order to clearly show its effect.

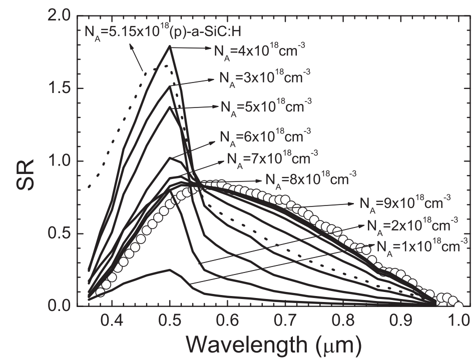

Fig. 6. SR as function of the boron doping density in the (p)-μc-Si:H layer. The SR of a device with a (p)-a-SiC:H layer with 0.47 eV activation energy is shown for comparison. The parameters of the defective layer are listed in Table 3. The cut-off wavelength λ_c of the optical low-pass filter was adopted as 710 nm. The experimental SR matched with the parameters of Table 2 is included for comparison purposes.

The dependence of the CPGE with respect the activation energy of the (n)-μc-Si:H was found to be very minor within the range 0.026 eV–0.43 eV.

5. Conclusions

The Complementary Photogating Effect (CPGE) refers to Spectral Responses (SR) greater than unity for short wavelengths of the probe beam in devices subjected to red bias illumination. The CPGE has not yet been reported in μc-Si:H based n-i-p devices optimized for photovoltaic applications. Using numerical simulations the conditions to observe the CPGE in μc-Si:H n-i-p devices were explored. SR higher than one for probe beam wavelengths approximately between 360 nm and 540 nm with its maximum at ~500 nm were predicted in μc-Si:H n-i-p junctions with an a-SiC:H p-doped layer when the buffer layer at the p/i interface has the following characteristics: density of defects between 6.8×10^{17} cm^{-3} and 2.2×10^{18} cm^{-3}, mobility gap wider than 1.55 eV and narrower than 2.23 eV, and thickness between 16 nm and 40 nm. The peak response was found to be sensitive to the cut-off wavelength of the optical low-band filter interposed between the bias light source and the sample. The maximum response (~2.46) was predicted for a cut-off wavelength of 730 nm assuming a 20 nm thick buffer layer with a defect density of 10^{18} cm^{-3} and a mobility gap of 1.85 eV. The CPGE is originated by the modulation of the positive charge trapped at donor-like states of the defective buffer layer by the a.c. short wavelength probe beam that consequently modulates the electric field and the recombination rates inside the intrinsic layer where recombination losses are most significant. When the short wavelength probe beam is shining in conjunction with the red bias light the recombination rate in the intrinsic layer is lower than when only the red bias light is illuminating the sample. Hence an effective net negative recombination rate or net gain is predicted inside the intrinsic layer when both the probe

beam and the bias light are simultaneously illuminating the sample and spectral responses higher than one are consequently obtained. The CPGE is predicted by D-AMPS in μc-Si:H based n-i-p devices with either high gap (a-SiC:H) or low gap (μc-Si:H) (p)-doped layers. In the second case the activation energy should be higher than the ones used in regular solar cells. The highest response is obtained for activation energies ~0.29 eV. Using appropriate long-pass optical filters peak values higher than 3 were predicted. The CPGE is also function of the capture cross sections of donor-like gap states and free carrier mobilities at the defective layer and at the front region of the intrinsic layer while it shows negligible or low dependence with respect to the n-layer activation energy, low probe beam intensities, and electrical parameters at the back region of the intrinsic layer. The μc-Si:H based solar cells with spectral responses greater than unity can be used as photodiodes with internal gain.

Acknowledgments

We highly appreciate the financial support of CONICET and Agencia Nacional de Promoción Científica y Tecnológica through the grants PIP-112-201101-01052 and PICT-2013 2098 respectively. I would also like to thank members of the department Photovoltaic Materials and Devices of Utrecht University, the Netherlands, for providing the experimental information, and to Eng. Marcelo de Greef for his help in fitting the experimental data and in preparing the figures.

References

[1] H.P. Maruska, M.C. Hicks, T.D. Moustakas, R. Froiedman, IEEE Trans. Electron Devices ED-31 (1984) 1343.
[2] P.J. McElheny, J.K. Arch, H.S. Lin, S.J. Fonash, J. Appl. Phys. 64 (1988) 1254.
[3] H. Hou, S.J. Fonash, Appl. Phys. Lett. 61 (1992) 186.
[4] F.A. Rubinelli, J. Appl. Phys. 75 (1994) 998.
[5] C. Main, J.H. Zollondz, S. Reynolds, W. Gao, R. Brüggemann, M.J. Rose, J. Appl. Phys. 85 (1999) 296.
[6] S.H. Bae, S.J. Fonash, J. Appl. Phys. 79 (1996) 2213.
[7] P. Chaterjee, J. Appl. Phys. 75 (1994) 1093.
[8] H. Li, R.E.I. Schropp, F.A. Rubinelli, J. Appl. Phys. 108 (2010) 014509.
[9] S. Reynolds, C. Main, V. Smirnow, A. Meftah, Phys. Status Solidi C 7 (3–4) (2010) 505.
[10] M. Gloeckler, J.R. Sites, J. Appl. Phys. 95 (2004) 4438.
[11] G. Agostinelly, D.L. Bätzner, M. Burgelman, Thin Solid Films 431–432 (2003) 407.
[12] F.A. Rubinelli, J.Y. Hou, S.J. Fonash, J. Appl. Phys. 73 (1993) 2548.
[13] F. Rubinelli, J. Rath, R. Schropp, J. Appl. Phys. 89 (2001) 4010.
[14] M.J. Powell, S.C. Deane, Phys. Rev. B 48 (1993) 10815.
[15] M. Van Veen, "Tandem solar cells deposited using hot-wire chemical vapor deposition", chapter 6, Ph.D Thesis in Natuur- en Sterrenkunde (Physics) at Utrecht University, 2003.
[16] J.K. Rath, C.H.M. van der Werf, F.A. Rubinelli, R.E.I. Schropp, Proceedings de 25th IEEE Photovoltaic Specialists Conference, Washington D.C., USA, 2, 1996 1101.
[17] J. Strenger, J.K. Rath, R.E.I. Schropp, F.A. Rubinelli, Thin Solid Films 501 (2006) 291.
[18] E. Klimovsky, J.K. Rath, R.E.I. Schropp, F.A. Rubinelli, Thin Solid Films 422 (2002) 211.
[19] M.W.M. van Cleef, J.K. Rath, F.A. Rubinelli, C.H.M. van der Werf, R.E.I. Schropp, W.F. van der Weg, J. Appl. Phys. 82 (1997) 6089.
[20] J.K. Arch, F. Rubinelli, J. Hou, S.J. Fonash, J. Appl. Phys. 69 (1991) 7057.
[21] J.M. Marshall, R.A. Street, J. Thompson, Philos. Mag. B 54 (1) (1986) 51.
[22] J.M. Marshall, R.A. Street, J. Thompson, W.B. Jackson, Philos. Mag. B 57 (3) (1988) 387.
[23] E.A. Schiff, J. Phys. Condens. Matter 16 (2004) S5265.
[24] L.C. Longeaud, J.A. Schmidt, R.R. Koropecki, Phys. Rev. B 73 (2006) 235317.
[25] T. Dylla, S. Reynolds, R. Carius, F. Finger, J. Non-Cryst. Solids 352 (2006) 1093.
[26] K.Y. Chan, D. Knipp, A. Gordijn, H. Stiebig, J. Appl. Phys. 104 (2008) 054506.
[27] T. Bronger, R. Carius, Thin Solid Films 515 (2007) 7486.